Nanomedicine: Nanotechnology, Biology, and Medicine xxx (xxxx) xxx

Contents lists available at ScienceDirect

Nanomedicine: Nanotechnology, Biology, and Medicine

journal homepage: www.sciencedirect.com/journal/nanomedicine-nanotechnology-biology-and-medicine

Investigating the mechanism of action of DNA-loaded PEGylated lipid nanoparticles

Luca Digiacomo, PhD [a], Serena Renzi, MSc [a], Erica Quagliarini, PhD [a], Daniela Pozzi, PhD [a], Heinz Amenitsch, PhD [b], Gianmarco Ferri, PhD [c], Luca Pesce, PhD [c], Valentina De Lorenzi, PhD [c], Giulia Matteoli, MSc [c], Francesco Cardarelli, PhD [c], Giulio Caracciolo, Prof. [a,*]

[a] NanoDelivery Lab, Department of Molecular Medicine, Sapienza University of Rome, 00161 Rome, Italy
[b] Institute of Inorganic Chemistry, Graz University of Technology, 8010 Graz, Austria
[c] Laboratorio NEST, Scuola Normale Superiore, 56127 Pisa, Italy

ARTICLE INFO

Keywords:
PEGylation, lipid nanoparticles
DNA delivery
Nanoparticle-membrane interactions

ABSTRACT

PEGylated lipid nanoparticles (LNPs) are commonly used to deliver bioactive molecules, but the role of PEGylation in DNA-loaded LNP interactions at the cellular and subcellular levels remains poorly understood. In this study, we investigated the mechanism of action of DNA-loaded PEGylated LNPs using gene reporter technologies, dynamic light scattering (DLS), synchrotron small angle X-ray scattering (SAXS), and fluorescence confocal microscopy (FCS). We found that PEG has no significant impact on the size or nanostructure of DNA LNPs but reduces their zeta potential and interaction with anionic cell membranes. PEGylation increases the structural stability of LNPs and results in lower DNA unloading. FCS experiments revealed that PEGylated LNPs are internalized intact inside cells and largely shuttled to lysosomes, while unPEGylated LNPs undergo massive destabilization on the plasma membrane. These findings can inform the design, optimization, and validation of DNA-loaded LNPs for gene delivery and vaccine development.

Background

Lipid nanoparticles (LNPs) represent a valuable platform for a variety of biomedical applications, especially for nucleic acid delivery. Compared to their virus-based counterparts, LNPs are easier to be manipulated/manufactured, less immunogenic, and thus safer at the clinical level.[1] Concerning manufacturing, the large-scale production of LNPs has extensively increased in the last decade thanks to technological advancements which enabled passing from conventional production procedures (e.g. by lipid film hydration) to automatized ones (i.e. by microfluidic mixing). The involvement of microfluidic devices allowed us to obtain small-sized and monodisperse LNPs in single-step protocols,[2,3] improving the reproducibility and scalability of the preparations. In 2018, the first LNP-based therapeutic nanosystem encapsulating siRNA molecules was approved by the Food and Drug Administration (FDA) and used for the treatment of polyneuropathy associated with hereditary variant transthyretin amyloidosis (ATTRv).[4,5] Starting from December 2020, the same technology was exploited to develop SARS-Cov2 vaccines (i.e. mRNA-encapsulating LNPs) and then effectively used to face the COVID-19 pandemic worldwide.[6] Of note, irrespective of the specific application, the LNP-surface functionalization with polyethylene glycol (PEG) is always employed. It is widely accepted that the presence of PEG on the outer surface of the LNP contributes to increasing its stability and retention time in circulation, while concomitantly reducing LNP proteolysis and renal excretion.[7] Overall, PEG contributes to reducing the frequency of vector administration. Based on the matter of facts, it is no surprise that FDA-approved mRNA-1273/SpikeVax by Moderna as well as BNT162b2/Comirnaty by BioNTech/Pfizer are PEGylated LNP systems.[5,8] At the same time, undesired immune-mediated side effects were associated with the presence of PEG on drug-delivery vectors.[9] For instance, the activation of the complement system, some hypersensitivity reactions, and an accelerated blood clearance (ABC) upon repeated administration[10,11] are thought to be triggered, to some extent, by the production of anti-PEG antibodies, which in turn trigger the recognition of PEGylated NPs by the immune system.[12] Noteworthy, side effects of PEGylation have been linked even to the occurrence of rare allergic reactions to COVID-19 vaccines.[9] Even at the cellular level,

* Corresponding author.
E-mail address: giulio.caracciolo@uniroma1.it (G. Caracciolo).

https://doi.org/10.1016/j.nano.2023.102697
Received in revised form 26 June 2023;
Available online 27 July 2023

the role of PEGylation remains controversial. For instance, while it was shown that PEG can create steric hindrance, resulting in significant inhibition of protein adsorption on the LNP surface and less recognition by macrophages, excessive PEGylation can lead to a strong inhibition of the overall process of cellular uptake, thus reducing the potential of the delivery system.[13] In this regard, it should be considered that effective delivery of therapeutic agents requires a successful overcoming of all the transfection barriers, including internalization, intracellular trafficking, endosomal escape, lysosomal accumulation, and nuclear entry.[14,15] In this work, we explored the effects of PEGylation on the intracellular behavior of LNPs by a combination of synchrotron small-angle X-ray scattering (SAXS), transfection experiments, and confocal microscopy followed by intracellular dynamics and colocalization analyses. To this end, we employed PEGylated cationic multicomponent LNPs encapsulating plasmid DNA. Plain (i.e. unPEGylated) LNPs with the same lipid composition and DNA-lipid mass ratio were used as a control. Concerning unPEGylated systems, the nanostructure of the PEGylated LNPs was more stable against disintegration by cellular membranes and this led to sensibly lower DNA release. This finding was supported by cellular experiments which demonstrated that PEGylated LNPs are internalized almost intact inside the cells, move fast, and are shuttled to the lysosomal compartment.

Methods

Materials

Zwitterionic lipids, dioleoyl phosphatidyl ethanol-amine (DOPE), and 1,2-dioleoyl-sn-glycero-3-phosphocholine (DOPC) with cationic lipids, 1,2-dioleoyl-3-trimethyl-ammonium-propane (DOTAP), and (3β-[N-(N′,*N*′-dimethyl-aminoethane)-carbamoyl])-cholesterol (DC-Chol), the anionic lipid 1,2-dioleoyl-sn-glycero-3-phospho-L-serine (DOPS) and the PEG-lipid 1,2-dioleoyl-sn-glycero-3-phosphoethanolamine-N-[amino(polyethylene glycol)-2000, were purchased from Avanti Polar Lipids (Alabaster, AL). Plasmid DNA (pmirGLO) coding for the firefly luciferase reporter gene was bought from Promega (Madison, WI, USA).

Preparation of LNPs

Cationic and zwitterionic lipids were used to obtain two different lipid nanoparticles (LNPs) prepared with and without PEG-lipid. All lipids were dissolved individually in absolute ethanol at a final concentration of 25 mM. The plain formulation was prepared using DOTAP: Dc-Chol: DOPC: DOPE: in a molar ratio of 25:25:25:25. The PEGylated formulation was prepared using DOTAP: Dc-Chol: DOPC: DOPE: DOPE-PEG in a molar ratio of 25:25:25:23.5:1.5. The molar concentration of DOPE-PEG used in this study was consistent with those employed in previous investigations.[16,17] pDNA was diluted in sodium acetate 25 mM at pH 4 to reach a final concentration of 0.4 mg/ml. The lipid and DNA solutions were mixed using the NanoAssemblr® Ignite™ microfluidic platform (Precision NanoSystems Inc., Vancouver, BC, Canada). This microfluidic platform comprises two syringes connected to a cartridge (Ignite NxGen) through separate inlets. The lipid and DNA solutions are combined under controlled conditions within the thin channel printed on the cartridge. We assembled LNPs at a total flow rate (TFR) of 2 ml/min, with a DNA-to-lipid flow rate ratio (FRR) equal to 3:1. After the micromixing the residual ethanol (25 % v/v) was eliminated through dialysis using a cassette with a molecular weight cut off (MWCO) of 3.5 kDa (Thermo Scientific, Rockford, AZ, USA) against 400 ml phosphate saline buffer (PBS) at pH = 7.4. The dialysis conditions were set according to literature[18] to provide complete ethanol removal from the sample solution. Finally, after 19 h of dialysis, the LNPs were collected in a sample tube and the final pH was measured with a pH meter.

Preparation of anionic liposomes

DOPS liposomes were prepared to be employed as a simplified model for biological membranes,[19] due to their anionic surface charge and abundant presence in the membranes of mammalian cells.[20] DOPS powder was dissolved in chloroform and placed for 4 h under a vacuum in a rotavapor to evaporate all the chloroform. The resulting lipid film was hydrated with water for 4 h to obtain a 5 mg/ml solution. The liposome formulation was then sonicated for 20 min with a tip sonicator in pulsed mode at 20 % intensity.

Size and zeta potential measurements

LNPs were diluted 1:10 with distilled water before the dynamic light scattering (DLS) analysis and 1:60 for the micro-electrophoresis. Zetasizer Nano ZS90 (Malvern, UK) was used to perform measurements. The size was shown as *Z*-average, intensity weighted hydrodynamic mean size of the particles. The results are reported as mean ± SD of three repeated measurements.

Encapsulation efficiency assay

The amount of encapsulated plasmid DNA (pDNA) (pmirGLO) in LNPs was evaluated through the Quanti-iT PicoGreen dsDNA assay kit (Thermo Fisher Scientific, Waltham, MA, USA). Reagents were prepared following the manufacturer's protocol, LNPs were diluted 150-fold in TE buffer and then placed in a 96-well plate (Corning ® 96Well solid polystyrene microplate, Sigma Aldrich, St. Luis, MI, USA). Samples were diluted two-fold with fluorescent reagent Quanti-iT Pico-Green. TritonX-100 (1 % v/v) was added to the wells to lyse the LNPs and measure the total DNA (i.e. sum of encapsulated DNA and free DNA). After 5 min of incubation at room temperature, the fluorescence was measured (475 nm excitation wavelength, 500–550 nm emission wavelength) using Glomax Discovery System (Promega, Madison, WI, USA). The following equation was used to calculate the LNPs encapsulation efficiency (EE):

$$EE(\%) = \frac{(\text{total DNA} - \text{free DNA})}{\text{total DNA}} x\ 100 \quad (1)$$

DNA release assay was performed using Quanti-iT PicoGreen dsDNA assay kit (Thermo Fisher Scientific, Waltham, MA, USA) to evaluate the free DNA on sample after the incubation of LNPs with anionic liposomes. LNPs were incubated for 1 h at room temperature with liposomes at 4 different lipid/lipid ratios (i.e. 0.05, 0.1, 0.5, and 1).

Synchrotron SAXS experiments

Synchrotron Small Angle X-ray Scattering (SAXS) measurements were performed at the Austrian SAXS beamline ELETTRA (Trieste, Italy),[21] with a Pilatus3 1 M (Dectris, Baden, Switzerland) detector, calibrated by using silver behenate powder (d-spacing = 5.838 nm). q-range was fixed in the range 0.05–5 nm^{-1}, with an exposure time of 10 s. Correction for background, primary beam intensity, and detector efficiency were included in the analysis. Finally, SAXS curves were fitted by a multi-Lorentzian function, according to the following equation:

$$I(q) = \sum_{i=1}^{M} \frac{A}{1 + i^2\left(\frac{q - q_{001}}{a}\right)^2} + \sum_{i=1}^{M} \frac{B}{1 + i^2\left(\frac{q - q_{002}}{b}\right)^2} + k \quad (2)$$

Where the first and the second term describe the first and the second Bragg's peak, located at q_{001} and q_{002}, with width proportional to a and b, and amplitude equal to A and B, respectively. Fitting procedures converged for M = 2.

Cell culture

Human embryonic kidney (Hek-293) cell line was bought from ATCC (Rockville,MD, USA) and maintained in Dulbecco's Modified Essential Medium (DMEM) enriched with 10 % v/v fetal bovine serum (FBS, Gibco Life Technologies) and 1 % v/v penicillin-streptomycin (Gibco Life Technologies). Cells were maintained in an incubator under a humidified atmosphere at 37 °C and 5 % CO_2.

Cell transfection

10^4 cells were seeded into 24 well plates in 500 μl of medium, DMEM supplemented with 10 % v/v FBS, 1 % v/v penicillin/streptomycin (PS) and incubated for 24 h at 37 °C and 5 % CO_2. After incubation, the media was replaced by 400 μl of Opti-MEM reduced serum medium containing LNPs for a final DNA concentration of 1 μg DNA per well. After 3 h of treatment, 400 μl of appropriate medium (i.e., DMEM) supplemented with 20%v/v FBS and 1 % v/v PS were added to each well. After 48 h of incubation at 37 °C and 5%CO_2 cells were washed with PBS and 60 μl Passive lysis Buffer (Promega) were added to each well. 10 μl of cell lysate were placed into 3 wells of a white 96-well plate and diluted with 100 μl of luciferase substrate reagent (Promega) while the remaining 30 μl were distributed (10 μl/well) into another 96-well plate for protein quantification, performed through BCA Assay Protein Kit (Thermo Fisher Scientific, Waltham, MA, USA). The transfection efficiency (TE) was expressed as relative light units (RLU) per mg of proteins.

Cell viability

10^4 cells were seeded into 96 well plates in 100 μl of DMEM supplemented with 10 % v/v FBS, 1 % v/v PS) and incubated 24 h at 37 °C and 5 % CO_2. After a day exhausted media was replaced by 100 μl of Opti-MEM reduced serum medium containing LNPs for a final DNA concentration of 0,25 μg DNA per well. After 3 h of treatment 100 μl of appropriate medium (i.e. DMEM) containing 20 % v/v FBS were added to each well and cells were incubated 48 h at 37 °C and 5 % CO_2. After the incubation half of the medium volume from each well was discarded and 50 μl of XTT prepared following the protocol was added. The absorbance was measured by Glomax Discover System (Promega, Madison, WI, USA) at 450 nm wavelength.

Confocal microscopy

Live-cell imaging experiments were performed with a Zeiss LSM 800 confocal microscope equipped with a 63×, 1.4 N.A. oil immersion objective, and GaAsP detectors. Approximately 2×10^5 HEK-293 cells were seeded in a WillCo glass bottom dish (22 mm) 24 h before the experiment. On the day of confocal acquisitions, cells were incubated with PEGylated or unPEGgylated LNPs labeled with TexasRed 1× for 3 h at 37°C. 30 min before confocal acquisition, cells were stained with LysoTracker DeepRed (ThermoFisher) for lysosome staining. A series of confocal acquisitions (512 × 512 pixels, 50 nm pixel size) were taken exciting TexasRed at 561 nm (HeNe laser) and the emission was collected in the 570–630 nm range. LysoTracker DeepRed was excited at 633 nm and emission was collected in the 650–750 nm range. To evaluate the colocalization level between LNPs and lysosomes Manders' and Pearson correlation coefficients were calculated using the JaCoP plugin for ImageJ software. To perform image Mean Square Displacement (iMSD) analysis, image time series of 400 frames were acquired (256 × 256 pixels, 100 nm pixel size, 0.2 s time lapse), then processed by custom scripts, as reported in previous works.[22–24] Briefly, the spatial-temporal correlation function of the detected intensity was computed and studied as a function of the lag-variables (i.e. two spatial and one temporal variable). The evolution of the Gaussian's variance σ^2 as a function of the lag-time represents the iMSD curve. This curve was fitted to

$$\sigma^2(\tau) = \sigma_0^2 + K\tau^{\alpha} \quad (3)$$

to determine the α-value, which is associated to subdiffusive (i.e. $\alpha < 1$), superdiffusive (i.e. $\alpha > 1$) motion, or Brownian diffusion (i.e. $\alpha = 1$). $\sigma_0{}^2$ represents the curve's intercept and is related to the average size of the fluorescent-labeled particles and the waist of the point spread function. Finally, to quantify the intracellular dynamics of the investigated systems, the iMSD curve was fitted to

$$\sigma^2(\tau) = \sigma_0^2 + 4D_M\tau + \frac{L^3}{3}\left(1 - exp\left\{-\frac{\tau}{\tau_c}\right\}\right) \quad (4)$$

Where where L defines the linear size of the confinement area, τ_c is an index of how fast confinement occurs, D_M is the particle diffusivity at large time scale and represents 1/4 of the derivative of σ^2 for $\tau \to \infty$.

Results

Characterization of LNPs was performed in terms of size, zeta potential, and nanostructure. As shown in Fig. 1a, size distributions of plain and PEGylated LNPs were slightly different from each other. Indeed, the average hydrodynamic diameter was about 140 nm for both formulations, but the plain LNP exhibited a larger polydispersity index than the PEGylated counterpart (Table 1).

Furthermore, both the LNPs were cationic and exhibited a high level of encapsulation efficiency, i.e. about 82 % and 77 % for plain and PEGylated systems, respectively (Table 1). This represents a promising achievement, considering the size and steric hindrance of the employed DNA (i.e. about 7350-bp plasmid). Despite manifold similarities between the two systems, differences in their zeta potential were detected (Fig. 1b). Indeed, plain LNPs carried a higher positive surface charge, leading to a zeta potential of about 52 mV, whereas for the PEGylated counterparts the measured average value was lower, reaching about 20 mV.

As a last step of the characterization analysis, we performed synchrotron SAXS measurements to assess the inner structure of LNPs. SAXS curves for plain and PEGylated LNPs are reported in Fig. 1 c. The corresponding fitting curves by multi-Lorentzian functions are shown as solid lines. In detail, experimental data were fitted according to Eq. 2 and exhibited two Bragg peaks located at $q_{001} \approx 0.92$ and $q_{002} \approx 1.85$. This indicates a spatial periodicity with a d-spacing $= 2\pi/q_{001} \approx 6.8$ nm, along the normal direction to the lipid bilayer. The extent of the d-spacing is compatible with the typical pattern of a lamellar lipid/DNA phase, with a repeat unit made of hydrated DNA molecules (of size about 2.5 nm) sandwiched between a lipid bilayer of thickness = 4 nm. By the measurement of the first-order peak's width (as the full width at half maximum), it is possible to estimate the spatial extent of the periodic domains (Debye-Sherrer relation), which reads $L_m = 2\pi/\Delta q \approx 42$ nm. Hence, the number of repeat units in the lipid/DNA domains of LNPs can be evaluated as $q_{001}/\Delta q \approx 6$. Taken together, the multi-Lorentizian shape, location, and width of Bragg's peaks suggest that the inner structures of unPEGylated and PEGylated systems were very similar, and consisted in locally ordered domains that were randomly oriented in different directions. Finally, cell transfection experiments indicated that both LNPs successfully delivered the encapsulated DNA to immortalized human embryonic kidney cells (Hek-293) cells, but with different efficiency. In detail, as reported in Fig. 1 d, e, plain LNPs exhibited significantly higher TE and slightly less biocompatibility than their PEGylated counterpart.

To elucidate which processes were responsible for the observed trends, we first evaluated the change in inner structure and the amount of released DNA from LNPs upon interactions with a membrane model. In detail, plain and PEGylated LNPs were exposed to increasing amounts of DOPS liposomes, which represented a simplified model for biological membranes.[19] DLS and microelectrophoresis were performed to assess the physical-chemical properties of DOPS liposomes that exhibited a

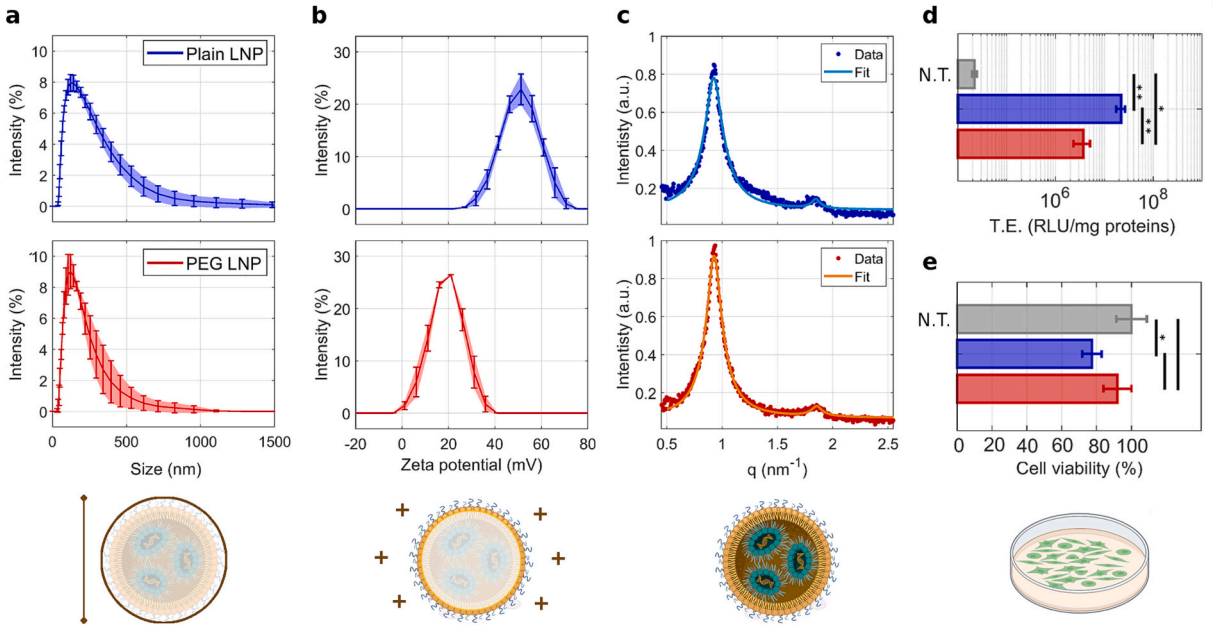

Fig. 1. Preliminary characterization. Physical-chemical characterization of (blue) plain and (red) PEGylated LNPs, in terms of (a) size, (b) zeta potential, and (c) nanostructure as determined by synchrotron SAXS. (d) Transfection efficiency (TE), and (e) cell viability of Hek-293 cells after 48-h treatments with LNPs. Not treated (N.T.) cells represent the negative control group, their corresponding data are depicted as grey bars. Statistical significance was evaluated by Student's t-test, and is indicated as follows: * $p < 0.05$; ** $p < 0.01$; no asterisk $p > 0.05$. As represented in the cartoon, at the end of these preliminary experiments, information about average diameter, surface charge, inner structure of LNPs, and biological response upon their administration in vitro was obtained. This cartoon was created using Biorender.com.

Table 1
Physical-chemical features of LNPs. Physical-chemical properties of plain and PEGylated LNPs, as obtained by dynamic light scattering, electrophoretic light scattering, Quanti-iT PicoGreen dsDNA assay kit, and synchrotron SAXS measurements.

	Average diameter (nm)	Polydispersity Index	Zeta potential (mV)	Encapsulation efficiency (%)	d-spacing (nm)	Domain size (nm)
Plain LNPs	138 ± 3	0.288 ± 0.019	52.0 ± 2.4	82.4 ± 1.6	6.78 ± 0.01	42.1 ± 1.3
PEGylated LNPs	132 ± 3	0.206 ± 0.017	19.7 ± 2.1	77.3 ± 2.4	6.80 ± 0.02	42.6 ± 2.5

size = 82 ± 2 nm and a zeta potential = −51 ± 3 mV. The choice of DOPS relies on its anionic surface charge and abundant presence in the membranes of mammalian cells,[20] which make it an optimal candidate to mimic membranes of cells and subcellular organelles. Synchrotron SAXS curves of LNP-DOPS systems are reported in Fig. 2 a, b, for each of the explored DOPS-to-LNP mass ratios, which is hereafter referred to as R. The typical multi-Lorentzian patterns of LNPs were preserved only at low R-values (i.e., R < 0.5), whereas became less prominent, or indistinguishable, at increasing higher DOPS amount (R ≥ 0.5). Although plain and PEGylated LNPs exhibited similar behaviors, their structural destabilization occurred differently. In fact, at the intermediate mass ratio (i.e. R = 0.5), plain systems were already destructured (Fig. 2a) whereas the first-order Bragg's peak was still present in the SAXS curve of the PEGylated counterparts (Fig. 2b), indicating greater particle stability. Finally, at R = 1 no Bragg's peak was detected for the plain LNPs, as a result of the total solubilization of the structure by DOPS molecules. However, a residual peak with very low prominence can be recognized for the PEGylated systems. This confirmed the lower tendency of PEGylated LNPs to be destabilized by lipid membranes. In addition, we evaluated the released DNA from LNPs as a function of R. Results are shown in Fig. 2c. The amount of encapsulated DNA decreased for both the investigated particles, but a steeper trend was detected for the unPEGylated LNPs. In detail, the percentage of encapsulated DNA started from about 80 % (i.e. encapsulation efficiency, at R = 0) and reached 10 % at R = 0.5. At equivalent values of R, the PEGylated systems consistently exhibited >50 % encapsulation of the gene cargo.

In addition to the interactions with membrane models, we studied the intracellular dynamics and final fate of LNPs in vitro, by performing FCS experiments, followed by iMSD analysis and quantitative colocalization with lysosomes. Green-labeled LNPs were administered to Hek-293 cells and followed in time. The output of the iMSD analysis of the acquired image time series is reported in Fig. 3a, as a function of the lag time τ. By evaluating the intercept, power-law, and asymptotic slope of the detected curves, information about the LNP dynamics can be obtained. In detail, the average size of fluorescent spots, type of motion, and diffusion coefficients are quantified by each of the aforementioned parameters, respectively. Results clearly indicate that the average size of fluorescent spots for plain LNPs was significantly higher than the PEGylated systems (Fig. 3b), their α-value close to one suggests a nearly Brownian diffusion (Fig. 3c), with a low diffusion coefficient (Fig. 3d). Conversely, small sized PEGylated particles (Fig. 3b) underwent a confined motion (α-value <1, Fig. 3c) with larger diffusion coefficients than the plain counterparts (Fig. 3d). In other words, PEGylated systems in cells were small, moved faster, but in a confined-diffusive way. On the other hand, plain LNPs exhibited larger sizes and moved slowly but with a lower degree of confinement. After assessing the intracellular dynamics of the systems, we focused on their final fate. To this end, we performed a colocalization analysis of green-labeled LNPs with red-labeled lysosomes. As shown by the representative image in Fig. 3 e, most of the plain LNPs were located at the cell membrane, and their green fluorescence signal was clearly distinguishable from the lysosomal one. Conversely, a large portion of PEGylated LNPs colocalized with lysosomes, as shown by the yellow spot-like structures in Fig. 3f. These considerations are quantitatively represented by the co-localization

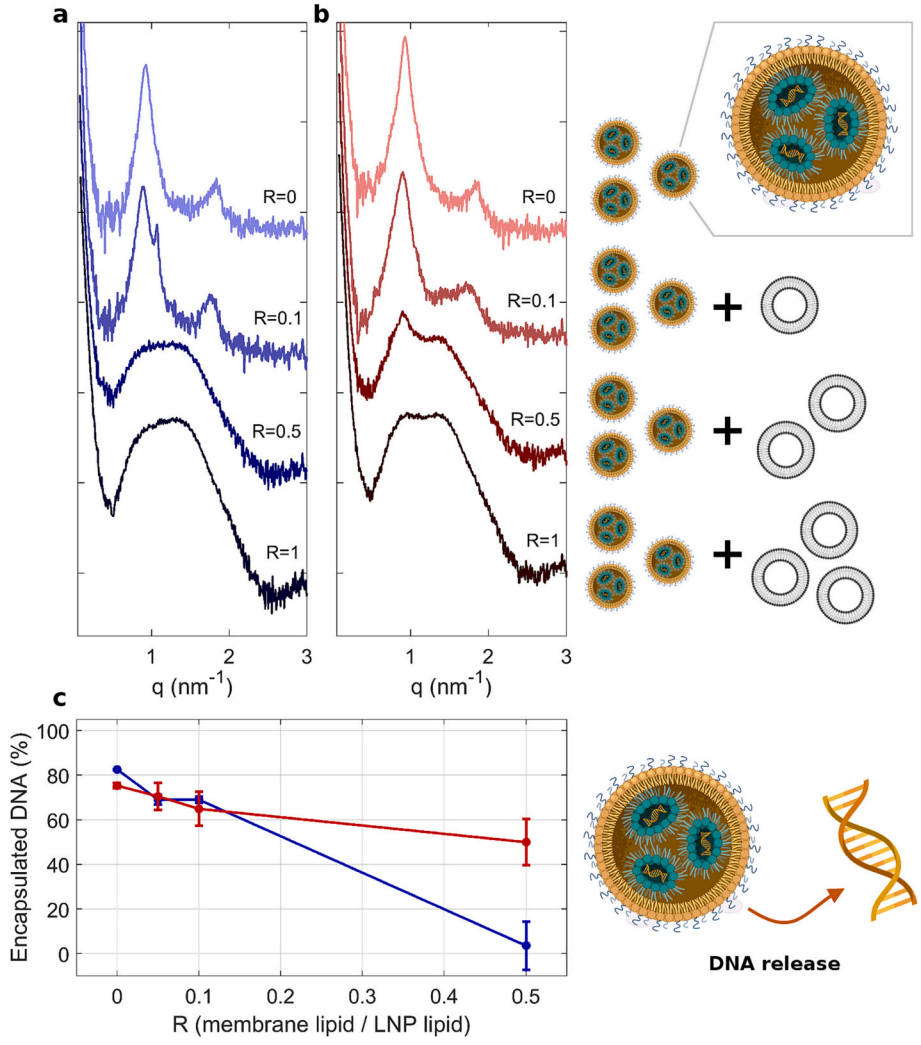

Fig. 2. Interactions of LNPs with membrane model. Effects of the interactions between LNPs and membrane model, at different membrane/LNP mass ratio R: (a, b) synchrotron SAXS data (curves are vertically shifted for clarity), and (c) loss of encapsulated DNA for (blue) plain and (red) PEGylated systems. The cartoon depicts the incubation of LNPs with different amounts of liposomes (grey) and the subsequent DNA release at large R values. This cartoon was created using Biorender.com.

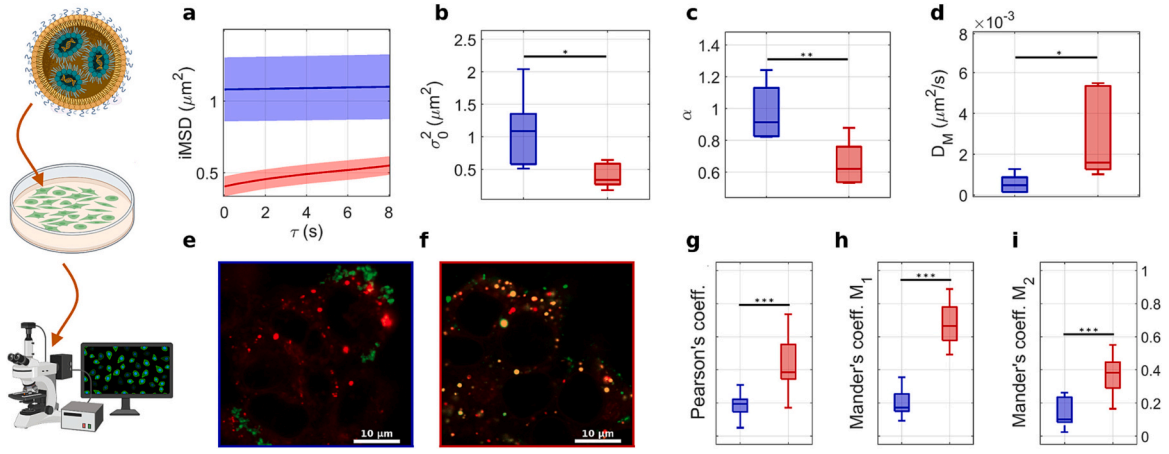

Fig. 3. Concofal microscopy analysis. As depicted in the cartoon, LNPs were administered to cells, then fluorescence confocal images were acquired and processed. (a) iMSD curve for (blue) plain and (red) PEGylated LNPs. Corresponding iMSD parameters are reported as (b) intercept σ_0,[2] (c) α-value from power-law trend, and (d) asymptotic diffusion coefficient D_M. Representative confocal images of green-labeled (e) plain LNPs and (f) PEGylated LNPs on Hek-293 cells. Red-labeled lysosomes are reported. (g) Pearson's, (h) Mander's M_1, and (i) Mander's M_2 coefficients obtained by quantitative colocalization analysis. Statistical significance was evaluated by Student's t-test and is indicated as follows: * $p < 0.05$; ** $p < 0.01$; ***$p < 0.001$; no asterisk $p > 0.05$. The cartoon was created using Biorender.com.

analysis performed on a dataset of 20 samples. Results are reported in Fig. 3 g-i, in terms of Pearson's and Mander's coefficients. Pearson's coefficient measures the pixel intensity correlation between green and red channels, whereas Mander's coefficient M_1 reports the portion of green pixels that colocalizes with the red ones. Similarly, Mander's coefficient $M2_2$ evaluates the portion of red pixels that colocalizes with the green ones. In our case, all the colocalization parameters exhibited the same trends and indicated clear and wide differences between the distributions corresponding to plain and PEGylated LNPs. Overall, the results obtained from FCS indicated that plain LNPs exhibited some degree of avoidance of lysosomal degradation, while PEGylated systems showed significant accumulation within lysosomes.

Discussion

Despite the latest clinical success achieved by PEGylated LNPs as a delivery system, little is still known about the role of PEGylation in modulating interactions and biological processes at cellular and subcellular levels. To get novel insights on this, here we investigated the mechanism of action of DNA-loaded PEGylated LNPs by a combination of gene reporter technologies, DLS, synchrotron SAXS, and FCS. The lipid composition used in this study was selected based on prior research conducted by our group. In those earlier investigations, we demonstrated that multicomponent lipoplexes with identical composition displayed remarkably high transfection efficiency in various cell lines, including cells that are typically difficult to transfect.[25–27] Then, after preparing unPEGylated and PEGylated LNPs by microfluidic mixing, we proceed with a preliminary characterization to assess their size, zeta potential and inner structure. Our outcomes revealed that the preparation procedure successfully resulted in uniform dispersions of particles with suitable size for clinical application. In fact, the size of nanocarriers is recognized as a key aspect that determines their clinical successes. For an instance, large particles hardly escape reticuloendothelial system (RES) uptake and are rapidly eliminated from blood circulation, whereas particles with size within 100–200 nm have a longer half-life and can reach target sites more easily (e.g. by the enhanced permeation and retention (EPR) effect).[28,29] Notably, the size of our LNPs perfectly fell in that range for both unPEGylated and PEGylated systems, whereas differences in their zeta potential were detected. UnPEGylated LNPs exhibited a higher cationic zeta potential than their unPEGylated counterparts. This trend is ascribable to the shielding effect of PEG molecules that are grafted on the surface,[30] and it has been reported in manifold works on different types of NP systems.[31–34] Synchrotron SAXS revealed the inner structure of the investigated systems. In detail, unPEgylated and PEGylated LNPs were very similar and presented locally ordered lipid/DNA domains that were randomly oriented in different directions. This random orientation with respect to the radial direction has been recently reported as a peculiar feature of LNPs,[35,36] and may represent one of the crucial points for the success of LNPs as delivery systems. Indeed, this spatial arrangement is less ordered than the typical multilamellar "onion-like" organization of lipoplexes.[37] Thus, it could be more easily disassembled upon interaction with cell membranes or subcellular compartments, with an efficient release of the molecular cargo in the cytoplasm, before that lipid degradation occurs. After such preliminary characterization, we measured the TE and cytotoxicity of the systems. The experiments revealed an inverse correlation between TE and biocompatibility of nanocarriers, in agreement with what has been observed for other lipid-based systems.[26] Such a trend represents a major concern for LNP design, as the goal would be the best compromise between efficiency and cytotoxicity. More interestingly, in our experiments, PEGylation hindered the TE of LNPs. Thus we wondered which processes and interactions were responsible for that observed behavior. To answer this question, we first evaluated the changes in inner structure and the amount of released DNA from LNPs upon interactions with a membrane model. Synchrotron SAXS experiments indicated a lower tendency of PEGylated LNPs to be destabilized by lipid membranes, whereas measurements on the encapsulated DNA confirmed that the structural destabilization of unPEGylated systems by DOPS membranes was responsible for a remarkable release of the loaded DNA. The structural stability of gene delivery systems is related to their in vitro efficiency, as it determines how the payload is delivered to the target sites. Low-stable systems generally lead to premature DNA release, but too-stable structures are responsible for DNA entrapment, poor nuclear entry, and limited gene expression.[38] In this regard, intracellular trafficking, endosomal escape, and lysosomal accumulation are so strongly interconnected to be considered as a single barrier to efficient delivery.[14] While these mechanisms have been deeply investigated for lipoplexes and polyplexes little is known for DNA-loaded LNPs.[39] In an attempt to address this issue, we administered LNPs to Hek-293 cells and performed FCS, followed by iMSD analysis[40] and quantitative colocalization with lysosomes. The former approach was used to characterize the intracellular dynamics of LNPs, in analogy with previous studies by some of us,[23,24] while the latter allowed us to quantify the lysosomal degradation of LNPs. Collectively, our findings suggest that the TE observed in plain LNPs can be attributed to two key factors. Firstly, their characteristic diffusive motion in the cell cytoplasm is a clear signature of scarce entrapment within subcellular organelles such as lysosomes,[14] thereby avoiding degradation. Secondly, plain LNPs possess the unique property of being readily disintegrated by cellular membranes, leading to a substantial release of the encapsulated DNA. In contrast, PEGylated LNPs demonstrate a restricted motion that is compatible with cytoskeleton-assisted transportation of particles toward the lysosomes,[14] where they undergo degradation. Based on colocalization analysis, it appears that a portion of PEGylated LNPs can escape from a final fate within lysosomes. We hypothesize that the structural stability of this particular fraction of PEGylated LNPs inhibits an effective release of DNA within the cytosol, thereby limiting the widespread distribution of the loaded DNA. In conclusion, we found that PEGylation endows LNPs with pronounced structural stability against disintegration by cellular lipids that, in turn, results in poor DNA release and large accumulation in lysosomes. This effect of PEGylation adds to other known unwanted effects (e.g. ABC effects and complement activation) and suggests that further approaches should be considered in the next future to overcome PEG limitations. These could involve the employment of PEG alternatives,[41] or the design of artificial biomolecular coronas,[42] which could simultaneously enhance the targeting properties of NPs and prevent adverse immune reactions.[43] We envision the mechanistic understanding of LNP-mediated cell transfection as being part of a future workflow for nanomedicine and other arenas in which biological interactions are relevant in view of a crosslinked classification of LNPs based on their biological properties and impact on cells.

Funding

This work was partly supported by the Italian Minister for University and Research (MUR) for the research project "TITAN" (Nanotecnologie per l'immunoterapia dei tumori) - Programma PON "R&I" 2014–2020 (ARS01_00906 to G.C.) and in part by the European Research Council (ERC) under the Horizon 2020 Programme (grant agreement No 866127 to F.C., project "CAPTUR3D").

CRediT authorship contribution statement

Luca Digiacomo: Data curation, Formal analysis, Investigation, Software, Validation, Visualization, Writing – original draft. **Serena Renzi:** Data curation, Formal analysis, Investigation, Validation, Visualization, Writing – original draft. **Erica Quagliarini:** Data curation, Formal analysis, Investigation, Validation. **Daniela Pozzi:** Conceptualization, Methodology, Project administration, Resources, Writing – review & editing. **Heinz Amenitsch:** Conceptualization, Methodology, Resources, Validation. **Gianmarco Ferri:** Investigation, Validation.

Luca Pesce: Investigation, Validation. **Valentina De Lorenzi:** Investigation, Validation. **Giulia Matteoli:** Investigation, Validation. **Francesco Cardarelli:** Conceptualization, Funding acquisition, Methodology, Project administration, Resources, Supervision, Writing – review & editing. **Giulio Caracciolo:** Conceptualization, Funding acquisition, Methodology, Project administration, Resources, Supervision, Writing – review & editing.

Acknowledgment

The authors acknowledge the CERIC-ERIC Consortium for the access to experimental SAXS facility.

References

1 Elsabahy M, Nazarali A, Foldvari M. Non-viral nucleic acid delivery: key challenges and future directions. *Curr Drug Deliv*. 2011;8(3):235–244.
2 Zhigaltsev IV, Belliveau N, Hafez I, Leung AK, Huft J, Hansen C, et al. Bottom-up design and synthesis of limit size lipid nanoparticle systems with aqueous and triglyceride cores using millisecond microfluidic mixing. *Langmuir*. 2012;28(7):3633–3640.
3 Leung AK, Tam YYC, Chen S, Hafez IM, Cullis PR. Microfluidic mixing: a general method for encapsulating macromolecules in lipid nanoparticle systems. *J Phys Chem B*. 2015;119(28):8698–8706.
4 Urits I, Swanson D, Swett MC, Patel A, Berardino K, Amgalan A, et al. A review of patisiran (ONPATTRO®) for the treatment of polyneuropathy in people with hereditary transthyretin amyloidosis. *Neurology and therapy*. 2020;9(2):301–315.
5 Akinc A, Maier MA, Manoharan M, Fitzgerald K, Jayaraman M, Barros S, et al. The Onpattro story and the clinical translation of nanomedicines containing nucleic acid-based drugs. *Nat Nanotechnol*. 2019;14(12):1084–1087.
6 Ndwandwe D, Wiysonge CS. COVID-19 vaccines. *Curr Opin Immunol*. 2021;71:111–116.
7 Veronese FM, Mero A. The impact of PEGylation on biological therapies. *BioDrugs*. 2008;22(5):315–329.
8 Guerrini G, Gioria S, Sauer AV, Lucchesi S, Montagnani F, Pastore G, et al. Monitoring anti-PEG antibodies level upon repeated lipid nanoparticle-based COVID-19 vaccine administration. *Int J Mol Sci*. 2022;23(16):8838.
9. de Vrieze, J., Suspicions grow that nanoparticles in Pfizer's COVID-19 vaccine trigger rare allergic reactions. *Science* 2020, *10* (10.1126).
10 Verhoef JJ, Carpenter JF, Anchordoquy TJ, Schellekens H. Potential induction of anti-PEG antibodies and complement activation toward PEGylated therapeutics. *Drug Discov Today*. 2014;19(12):1945–1952.
11 Mohamed M, Abu Lila AS, Shimizu T, Alaaeldin E, Hussein A, Sarhan HA, et al. PEGylated liposomes: immunological responses. *Science and Technology of Advanced Materials*. 2019;20(1):710–724.
12 Tian Y, Gao Z, Wang N, Hu M, Ju Y, Li Q, et al. Engineering poly (ethylene glycol) nanoparticles for accelerated blood clearance inhibition and targeted drug delivery. *J Am Chem Soc*. 2022;144(40):18419–18428.
13 Zalba S, Ten Hagen TL, Burgui C, Garrido MJ. Stealth nanoparticles in oncology: facing the PEG dilemma. *J Control Release*. 2022;351:22–36.
14 Cardarelli F, Digiacomo L, Marchini C, Amici A, Salomone F, Fiume G, et al. The intracellular trafficking mechanism of Lipofectamine-based transfection reagents and its implication for gene delivery. *Sci Rep*. 2016;6(1):25879.
15. Pozzi D, Marchini C, Cardarelli F, Salomone F, Coppola S, Montani M, et al. Mechanistic evaluation of the transfection barriers involved in lipid-mediated gene delivery: interplay between nanostructure and composition. *Biochimica et Biophysica Acta (BBA)-Biomembranes*. 2014;1838(3):957–967.
16 Algarni A, Pilkington EH, Suys EJ, Al-Wassiti H, Pouton CW, Truong NP. In vivo delivery of plasmid DNA by lipid nanoparticles: the influence of ionizable cationic lipids on organ-selective gene expression. *Biomater Sci*. 2022;10(11):2940–2952.
17 Sinegra AJ, Evangelopoulos M, Park J, Huang Z, Mirkin CA. Lipid nanoparticle spherical nucleic acids for intracellular DNA and RNA delivery. *Nano Lett*. 2021;21(15):6584–6591.
18 Swart L, Koekman C, Seinen C, Issa H, Rasouli M, Schiffelers R, et al. A robust post-insertion method for the preparation of targeted siRNA LNPs. *Int J Pharm*. 2022;620,121741.
19 Pozzi D, Caracciolo G, Caminiti R, De Sanctis SC, Amenitsch H, Marchini C, et al. Toward the rational design of lipid gene vectors: shape coupling between lipoplex and anionic cellular lipids controls the phase evolution of lipoplexes and the efficiency of DNA release. *ACS Appl Mater Interfaces*. 2009;1(10):2237–2249.
20 Gahan CG, Van Lehn RC, Blackwell HE, Lynn DM. Interactions of bacterial quorum sensing signals with model lipid membranes: influence of membrane composition on membrane remodeling. *Langmuir*. 2022;39(1):295–307. ACS Publications.
21 Amenitsch H, Rappolt M, Kriechbaum M, Mio H, Laggner P, Bernstorff S. First performance assessment of the small-angle X-ray scattering beamline at ELETTRA. *J Synchrotron Radiat*. 1998;5(3):506–508.
22 Ferri G, Digiacomo L, D'Autilia F, Durso W, Caracciolo G, Cardarelli F. Time-lapse confocal imaging datasets to assess structural and dynamic properties of subcellular nanostructures. *Scientific Data*. 2018;5(1):1–8.
23 Digiacomo L, D'Autilia F, Durso W, Tentori PM, Caracciolo G, Cardarelli F. Dynamic fingerprinting of sub-cellular nanostructures by image mean square displacement analysis. *Sci Rep*. 2017;7(1):14836.
24 Digiacomo L, Digman MA, Gratton E, Caracciolo G. Development of an image mean square displacement (iMSD)-based method as a novel approach to study the intracellular trafficking of nanoparticles. *Acta Biomater*. 2016;42:189–198.
25 Caracciolo G, Pozzi D, Amenitsch H, Caminiti R. Multicomponent cationic lipid–DNA complex formation: role of lipid mixing. *Langmuir*. 2005;21(25):11582–11587.
26 Giulimondi F, Vulpis E, Digiacomo L, Giuli MV, Mancusi A, Capriotti AL, et al. Opsonin-deficient nucleoproteic corona endows unPEGylated liposomes with stealth properties in vivo. *ACS Nano*. 2022;16(2):2088–2100.
27. Palchetti S, Pozzi D, Marchini C, Amici A, Andreani C, Bartolacci C, et al. Manipulation of lipoplex concentration at the cell surface boosts transfection efficiency in hard-to-transfect cells. *Nanomedicine: Nanotechnology, Biology and Medicine*. 2017;13(2):681–691.
28 Bozzuto G, Molinari A. Liposomes as nanomedical devices. *Int J Nanomedicine*. 2015;10:975.
29 Fanciullino R, Ciccolini J. Liposome-encapsulated anticancer drugs: still waiting for the magic bullet? *Curr Med Chem*. 2009;16(33):4361–4373.
30 Thi Nguyen N-T, Yun S, Lim DW, Lee E. Shielding effect of a PEG molecule of a mono-PEGylated peptide varies with PEG chain length. *Preparative Biochemistry and Biotechnology*. 2018;48(6):522–527.
31 Okuda T, Kawakami S, Maeie T, Niidome T, Yamashita F, Hashida M. Biodistribution characteristics of amino acid dendrimers and their PEGylated derivatives after intravenous administration. *J Control Release*. 2006;114(1):69–77.
32 Zhang X, Pan SR, Hu HM, Wu GF, Feng M, Zhang W, et al. Poly (ethylene glycol)-block-polyethylenimine copolymers as carriers for gene delivery: effects of PEG molecular weight and PEGylation degree. *Journal of Biomedical Materials Research Part A: An Official Journal of The Society for Biomaterials, The Japanese Society for Biomaterials, and The Australian Society for Biomaterials and the Korean Society for Biomaterials*. 2008;84(3):795–804.
33 Wolfram J, Suri K, Yang Y, Shen J, Celia C, Fresta M, et al. Shrinkage of pegylated and non-pegylated liposomes in serum. *Colloids Surf B Biointerfaces*. 2014;114:294–300.
34 Pozzi D, Colapicchioni V, Caracciolo G, Piovesana S, Capriotti AL, Palchetti S, et al. Effect of polyethyleneglycol (PEG) chain length on the bio–nano-interactions between PEGylated lipid nanoparticles and biological fluids: from nanostructure to uptake in cancer cells. *Nanoscale*. 2014;6(5):2782–2792.
35 Cui L, Renzi S, Quagliarini E, Digiacomo L, Amenitsch H, Masuelli L, et al. Efficient delivery of DNA using lipid nanoparticles. *Pharmaceutics*. 2022;14(8):1698.
36 Quagliarini E, Renzi S, Digiacomo L, Giulimondi F, Sartori B, Amenitsch H, et al. Microfluidic formulation of DNA-loaded multicomponent lipid nanoparticles for gene delivery. *Pharmaceutics*. 2021;13(8):1292.
37 Marchini C, Pozzi D, Montani M, Alfonsi C, Amici A, Amenitsch H, et al. Tailoring Lipoplex composition to the lipid composition of plasma membrane: a Trojan horse for cell entry? *Langmuir*. 2010;26(17):13867–13873.
38 Caracciolo G, Marchini C, Pozzi D, Caminiti R, Amenitsch H, Montani M, et al. Structural stability against disintegration by anionic lipids rationalizes the efficiency of cationic liposome/DNA complexes. *Langmuir*. 2007;23(8):4498–4508.
39 Quagliarini E, Wang J, Renzi S, Cui L, Digiacomo L, Ferri G, et al. Mechanistic insights into the superior DNA delivery efficiency of multicomponent lipid nanoparticles: an in vitro and in vivo study. *ACS Appl Mater Interfaces*. 2022;14(51):56666–56677. ACS Publications.
40. Di Rienzoa C, Grattonc E, Beltrama F, Cardarellia F. Fast spatiotemporal correlation spectroscopy to determine protein lateral diffusion laws in live cell membranes. *PNAS*. 2013;110(30):12307–12312.
41 Hoang Thi TT, Pilkington EH, Nguyen DH, Lee JS, Park KD, Truong NP. The importance of poly (ethylene glycol) alternatives for overcoming PEG immunogenicity in drug delivery and bioconjugation. *Polymers*. 2020;12(2):298.
42 Giulimondi F, Digiacomo L, Pozzi D, Palchetti S, Vulpis E, Capriotti AL, et al. Interplay of protein corona and immune cells controls blood residency of liposomes. *Nat Commun*. 2019;10(1):1–11.
43 Digiacomo L, Pozzi D, Palchetti S, Zingoni A, Caracciolo G. Impact of the protein corona on nanomaterial immune response and targeting ability. *Wiley Interdiscip Rev Nanomed Nanobiotechnol*. 2020;12(4), e1615.